Supplemental Figure Legends

Fig. S1. Validation of laser capture microdissection transcriptional analyses of the chicken DM. In situ hybridization at HH21, using indicated probes. Scale bars: 50 μm.

Fig. S2. Live imaging setup for time lapse of transient D-V cords and TUNEL assay. A Tie-1 H2B-YFP transgenic quails with wholemount view (**B**) of D-V endothelial cords. **C** Embryos are sliced into 150 μm transverse sections and then (**D**) embedded in low melting point agarose for imaging on glass-bottom culture plates. **E** Example of YFP fluorescent tissue slice, showing bilateral (left panel) and left-sided (right panel) endothelial cords; these panels are simplified in a cartoon model (**G**). (**H-J**) TUNEL assay of Tie-1 H2B-YFP transgenic quails demonstrating in **H** the absence of TUNEL-positive cells (red) in the DM and in Tie-1 H2B-YFP expressing endothelial cells (green, arrowhead); TUNEL-positive cells in the apoptotic mesonephros (MSN, boxed region of **H** is magnified in **I**) and in the limb bud AER (apical ectodermal ridge, **J**, from the same embryo as **H**).

Fig. S3. Analysis of arterial vasculogenesis in chicken and mice. Asymmetric formation of D-V cords in mice at E.10.75 (*Gja5*). Scale bar: 50 μm.

Fig. S4. Analysis of Cxcr4/Cxcl12 expression downstream of Pitx2. A ISH at HH14 (chicken) reveals *Cxcr4* expression (**left panel**) in Tie1-expressing (H2B-YFP, **right panel**) endothelial cells of the bilateral intervening plexus (black arrowheads). **B** Later, Cxcr4 expression is found both in the 1^0LA and gut plexus, but not the CMA. **C**, Misexpression of Pitx2/GFP in the right DM (right panel GFP marks electroporated cells) causes left isomerism ("double-left"

phenotype) including double *Cxcr4*-positive arterial cords (orange arrowheads) and duplicated 1^0LA (red arrows). **D** Loss of *Cxcl12* expression in the DM of *Pitx2*-/- mouse (E12.0), with left lateral (**top two rows**) and transverse views shown (**third row**). Positive control tissue from matched embryos (**bottom row**) reveals Cxcl12 staining in the scleratome. **E** Pitx2 binding at vascular network genes in vivo. (**1-2**) 5 enriched Pitx2 binding peaks surround *Cxcl12* (**1**), one of which directly overlaps with exon 1 on *Cxcl12* (**2**). (**3-4**) No significant Pitx2 binding is observed at the *Cxcr4* locus, the promoter of the adjacent gene *Dars* contains an enriched peak (**3**) but no peaks are observed in the promoter proximal region of *Cxcr4* (**4**). ChIP-seq data derive from published transgenic FLAG-tagged Pitx2 binding in 12-week mouse cardiac tissue (NCBI Gene Expression Omnibus (GEO) data repository accession GSE50401): top green track shows normalized ChIP-seq tag numbers (y-axis) and the user supplied track below shows peaks with at least 4-fold enrichment over input control indicated as vertical black bars. RefSeq gene models are indicated in blue, while bottom track shows PhastCons vertebrate conservation score in green. Scale bars: **A** 50 μm; **B** 100 μm.

Fig. S5. Side-specific effects of AMD3100 inhibitor-soaked beads on *Pitx2* expression and DM morphology. AMD3100 has no effect on normal left-sided *Pitx2* expression (**left panel**) or cellular morphology (**right panel**) of the DM. Scale bars: 50 μm.

Fig. S6. Cxcl12 is not sufficient to drive vessel formation in the absence of *Pitx2*. A Misexpression of Cxcl12 (pCAG-Cxcl12/pCAG-GFP) on the right side via co-electroporation produces normal L-R DM cellular morphology (fast green), results in ectopic levels of Cxcl12 that exceed those on the left side (ISH, *Cxcl12*), and is not sufficient to promote formation of

ectopic D-V cords in the right DM (ISH, *Gja5*, black dashed box). **B** Results of left-sided and right-sided targeting of Cxcl12 in the DM at HH21 (ISH, *Gja5*, model cartoon included). Transverse views shown to appreciate L-R situs and lateral view (Cranial-Caudal) to appreciate the extent of 1^0LA formation. (**1**) Wild type DM showing left-sided D-V cord (orange arrowhead) and 1^0LA formation (red arrow). (**2**) 'Double-left' phenotype with right-sided Pitx2 electroporation (GFP) showing left- and right-sided D-V cords and two 1^0LA. (**3**) Right-sided Cxcl12 electroporation (GFP) showing ectopic 1^0LA forming on the right side as a result of accelerated remodeling of the left-sided, Cxcr4-positive (**4**) D-V cords (see also Fig. 6). This result is in contrast to (**2**) highlighting an important functional difference between Pitx2 and Cxcl12 in the DM. (**5**) Left-sided Cxcl12 electroporation (GFP) showing accelerated formation of 1^0LA as a result of accelerated remodeling of the left-sided D-V cords. **C** The diffusion range of AMD3100 inhibitor does not allow it to cross the midline boundary of the DM: inhibitor beads placed on the right side (**middle panel**, right lateral view) have no effect on the normal left-sided assembly of endothelial cords (**right panel,** arrowhead) and 1^0LA (**left panel**, arrow). Bead positions are indicated. Scale bars: **A-B** 50 μm; **C** 100 μm.

Fig. S7 Lymphatic marker expression in tissues surrounding the DM. A Prox1-GFP-marked lymphatic anlagen in the retroperitoneal lymph sac (RLS), caudal cardinal veins (CCV) and non-lymphatic staining in the sympathetic trunk (ST) and neural tube (NT). **B** Adjacent transverse sections showing that location of lymphatic anlagen (green arrows) in three different HH27 chicken embryos, marked by *Prox1* (**left column**) and *Vegfr3* (**middle column**) is spatially distinct from *Prox1*-expressing cells of the avian-specific Nerve of Remak (Hnk1-positive, **right column**). **C Top row** Wholemount (left) and transverse views (right) of wild type mouse DM

stained with anti-Prox1; lymphatic plexus is first visible ventrally (white arrows, higher magnification inset) that extends dorsally. **Bottom row** Absence of Prox1-GFP reporter signal in mouse cranial or caudal DM prior to E10.5, revealed by transverse section of E10 Prox1 transgenic reporter mice. Scale bars: **A-B** 50 μm.

Fig. S8 Local lymphangiogenesis in the left DM requires the preceding Pitx2-driven arterial program. A *Vegfr3* expression (ISH) is absent from *Pitx2*-/- mutant DM at E13.5 but remains unchanged along the CMA. **B**, Cxcr4/Cxcl12-inhibiting AMD3100 beads (**right panel**) on the left side of the chicken DM abrogate the *Lyve1*-positive network (HH23), compared to PBS beads (**left panel**). **C** Wholemount double immunohistochemistry for Prox1 (green) and PECAM/CD31 (red) reveals loss of Prox1 staining (asterisk) in the DM of Cxcr4 -/- mutant mouse embryos at E13.5 (**middle panel**) compared to wild type littermates (**left panel**). Peripheral limb lymphatics are unchanged in matched embryos (**right column**). **D** Arteriogenesis-inhibiting Quinidine beads on the left side of the chicken DM have no effect on *Cxcl12* expression (HH21). Scale bars: **A** 50 μm; **B-D** 50 μm.

Movie S1. **Right-sided endothelial cord regression in midgut explants of Tie-1-H2B-eYFP quail embryos. Left panel:** Select nuclei of endothelial cells of right DM were manually tracked with dragon tails (Bitplane Imaris software). **Right panel**: Tracking of select endothelial nuclei of the left cord (green), right cord (red) and dorsal aorta (blue). At time T=0 (HH17, 60 hours), bilateral endothelial cords are present in the DM. At T=4.5 hours (HH18, 65 hours), cells of the right side endothelial cords have significantly regressed and by T=6.5 hours (HH19, 70.5 hours) the regression is complete.

Movie S2. Right to left endothelial cell migration in midgut explants of Tie-1-H2B-eYFP quail embryos. Left panel: Select nuclei of endothelial cells of right DM were manually tracked with dragon tails (Bitplane Imaris software). **Right panel**: Tracking of select endothelial nuclei of the left cord (green), right cord (red) and dorsal aorta (blue). Starting at HH19, time-lapse imaging reveals that cells within right-sided endothelial cords regress, migrate and anastomose with the left endothelial cords giving rise to vasculature asymmetries in the DM.

Movie S3: Complete regression and endothelial cell emigration of right-sided arterial cord. Left panel: Time-lapse of Tie-1 H2B-eYFP quail embryo midgut explants shows remodeling of the intervening endothelial plexus to yield the left DV arterial cord. At time T =0 (HH17), bilateral endothelial cords are present in the DM. At T=5 hours (HH18), cells of the right side endothelial cords have significantly regressed and by T=10.5 hours (HH19) regression is complete. By T =13.5 hours (HH20) we find that regressed cells from the right migrate left and contribute to the left endothelial cord. **Right panel:** Select nuclei of endothelial cells of the left and right cord, and left and right dorsal aortae are labeled with green, red, purple and blue spots, respectively; tracking of these spots models the cell movements in the left panel movie.

Fig. S1

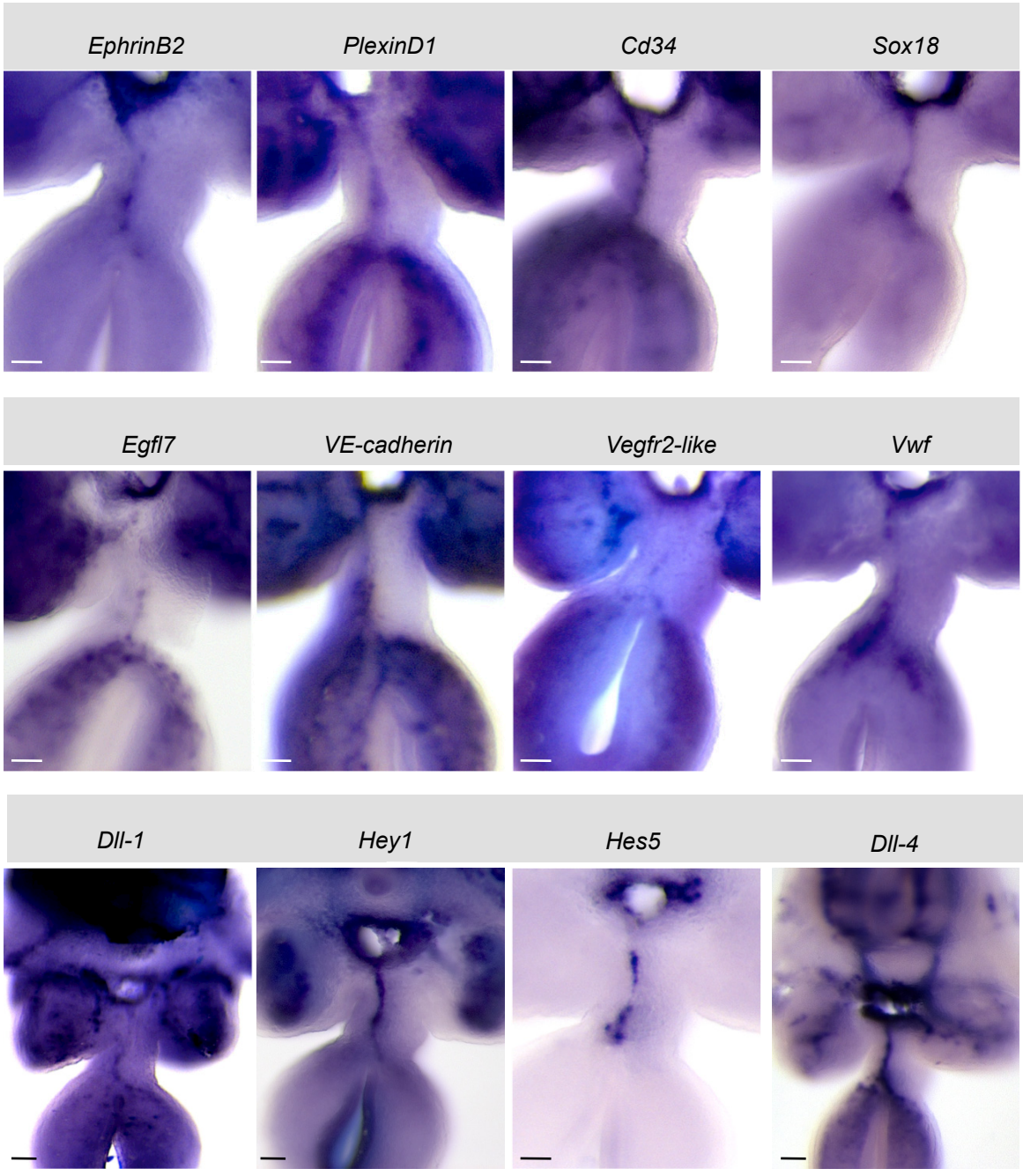
EphrinB2
PlexinD1
Cd34
Sox18
Egfl7
VE-cadherin
Vegfr2-like
Vwf
Dll-1
Hey1
Hes5
Dll-4

Fig. S2

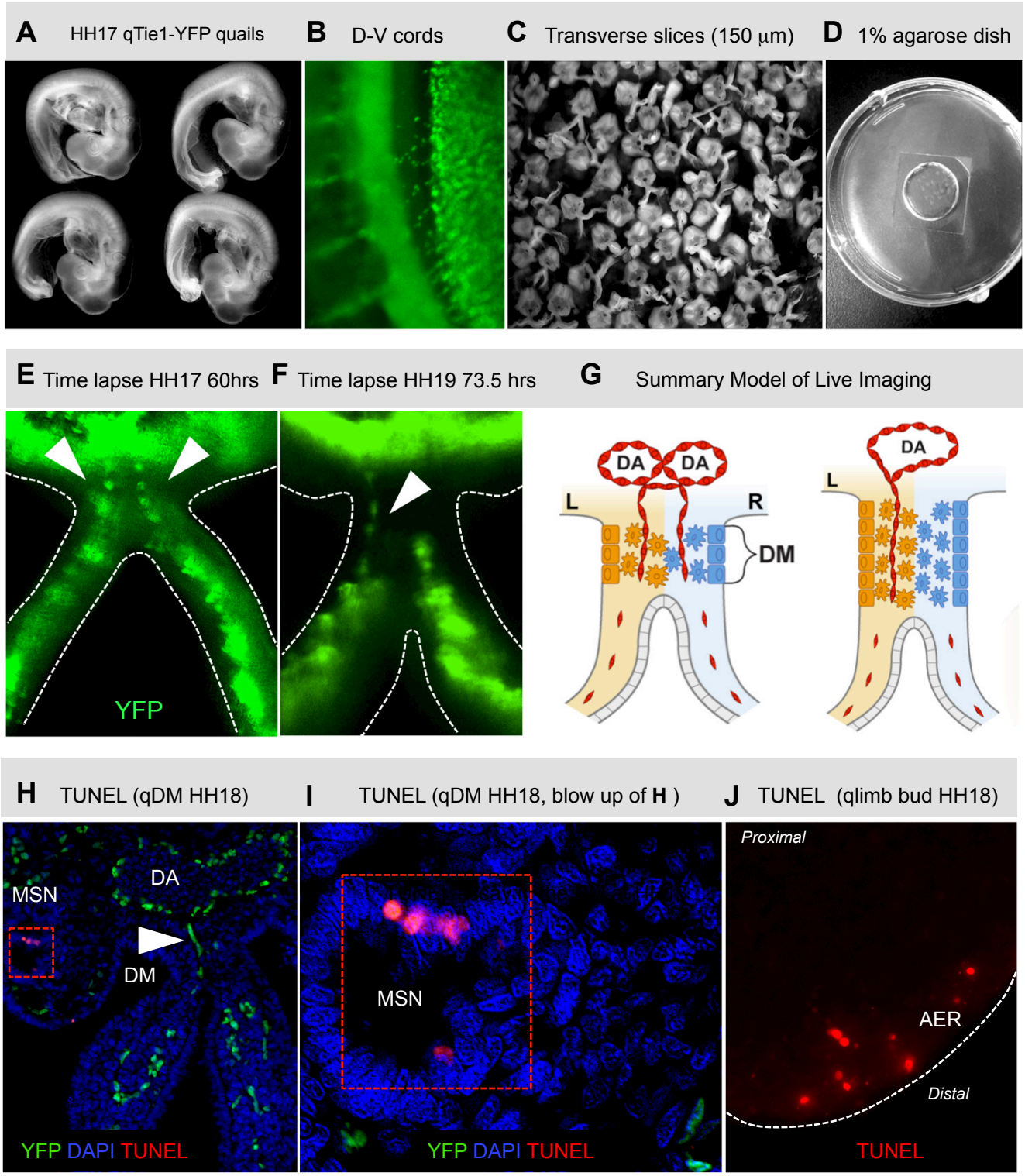
A HH17 qTie1-YFP quails
B D-V cords
C Transverse slices (150 μm)
D 1% agarose dish
E Time lapse HH17 60hrs
F Time lapse HH19 73.5 hrs
G Summary Model of Live Imaging
YFP
DA
DA
L
R
DM
DA
L
H TUNEL (qDM HH18)
I TUNEL (qDM HH18, blow up of H)
J TUNEL (qlimb bud HH18)
MSN
DA
DM
YFP DAPI TUNEL
MSN
YFP DAPI TUNEL
Proximal
AER
Distal
TUNEL

Fig. S3

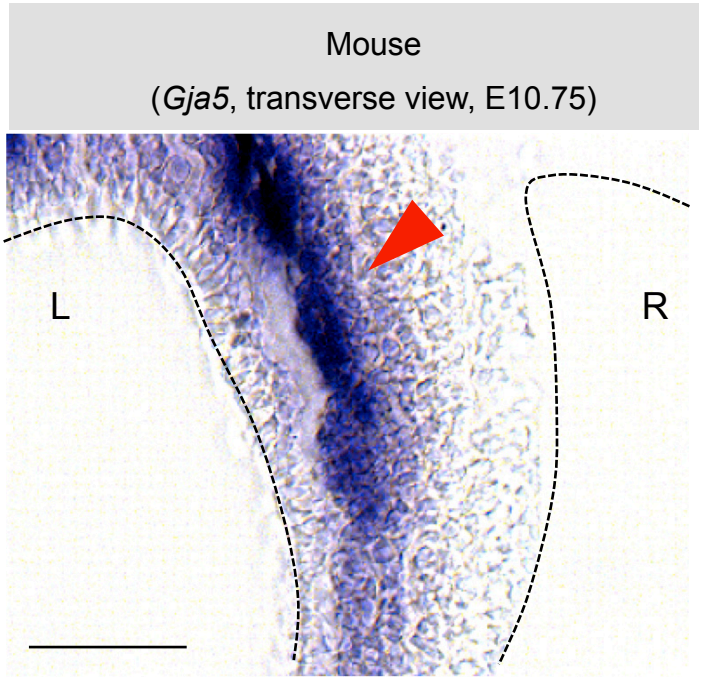

Fig. S4

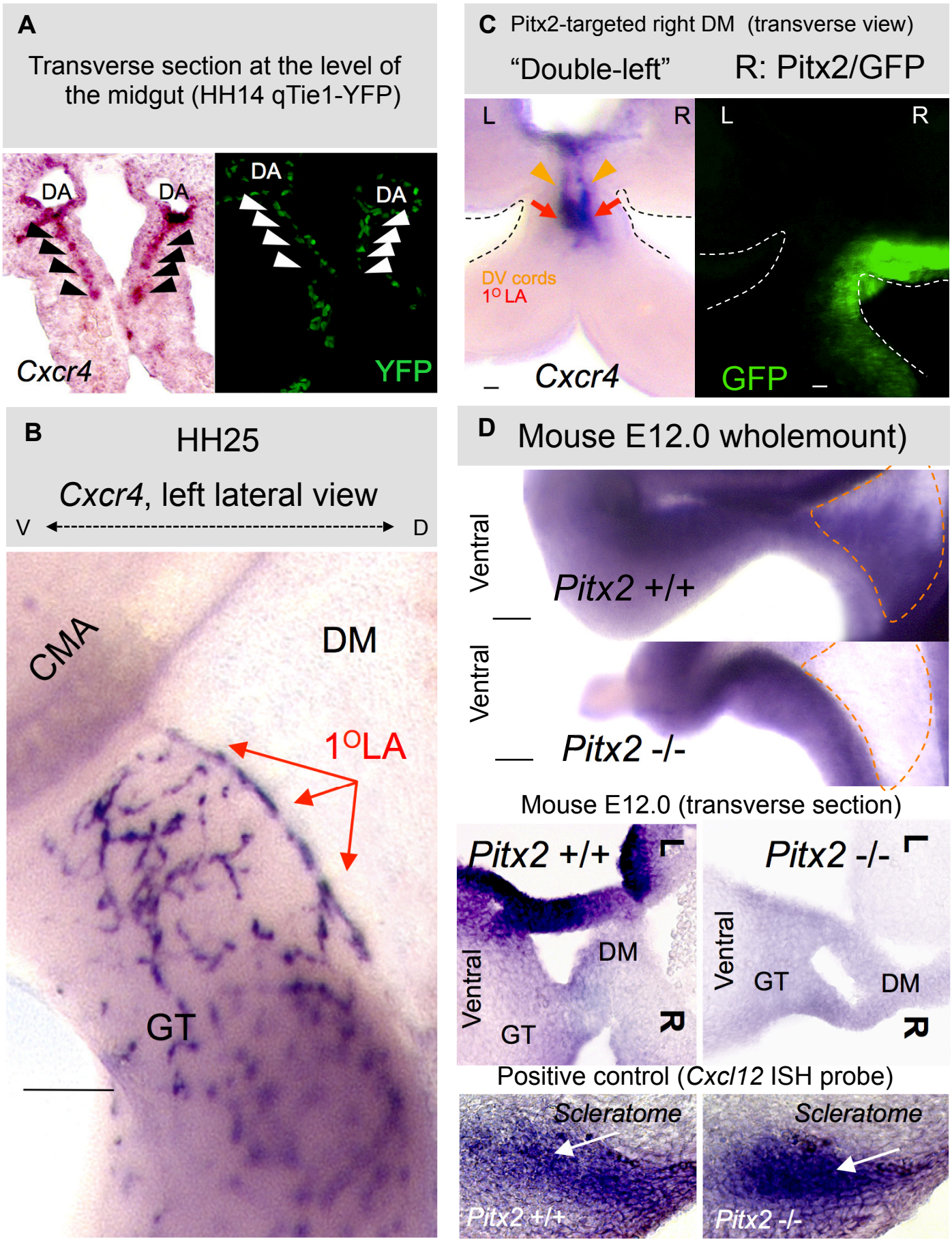
A
Transverse section at the level of the midgut (HH14 qTie1-YFP)
DA
DA
DA
DA
Cxcr4
YFP
B
HH25
Cxcr4, left lateral view
V
D
CMA
DM
1°LA
GT
C Pitx2-targeted right DM (transverse view)
"Double-left"
R: Pitx2/GFP
L
R
L
R
DV cords
1° LA
Cxcr4
GFP
D Mouse E12.0 wholemount)
Ventral
Pitx2 +/+
Ventral
Pitx2 -/-
Mouse E12.0 (transverse section)
Pitx2 +/+
DM
Ventral
GT
R
Pitx2 -/-
Ventral
GT
DM
R
Positive control (Cxcl12 ISH probe)
Scleratome
Pitx2 +/+
Scleratome
Pitx2 -/-

Fig. S4

E Pitx2 binding at vascular network genes in vivo

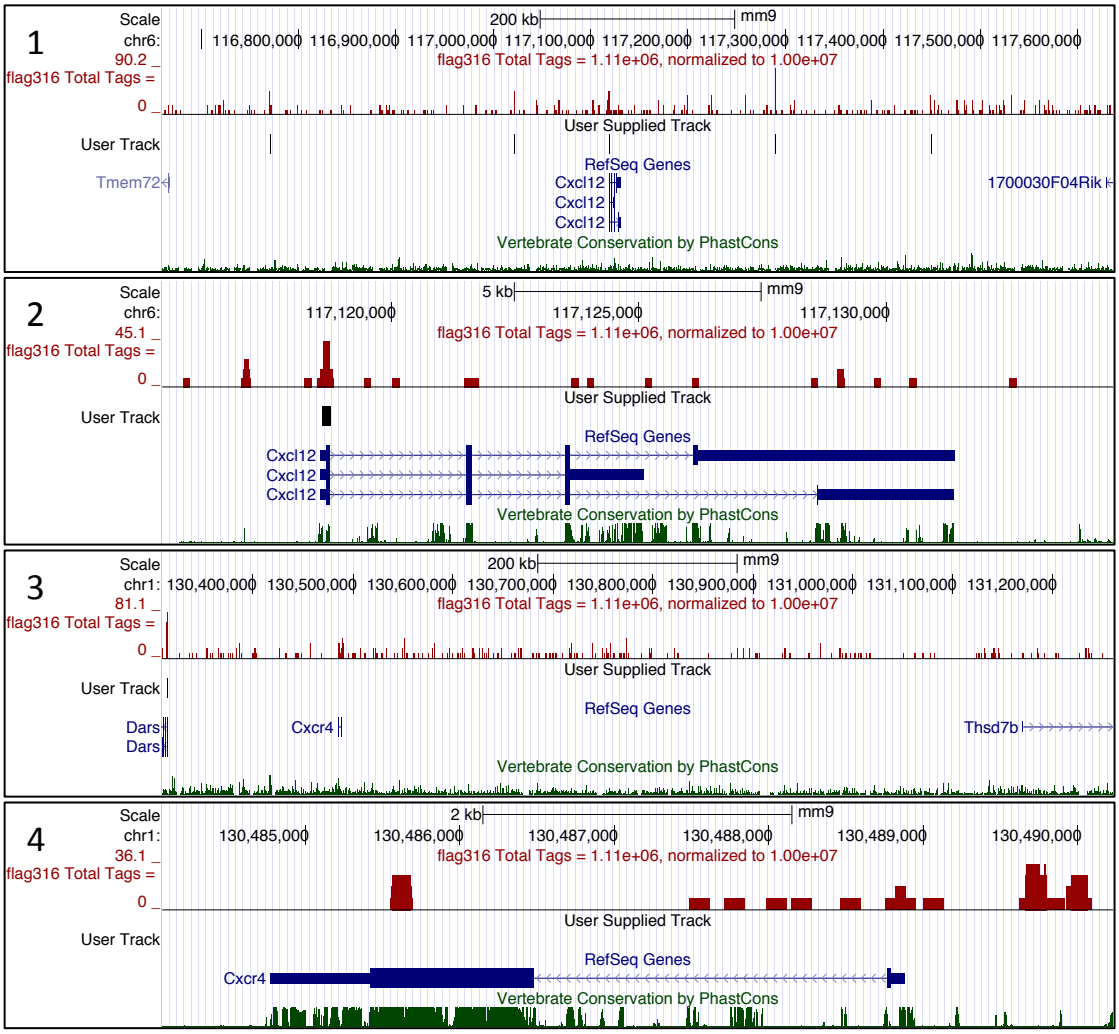

Fig. S5

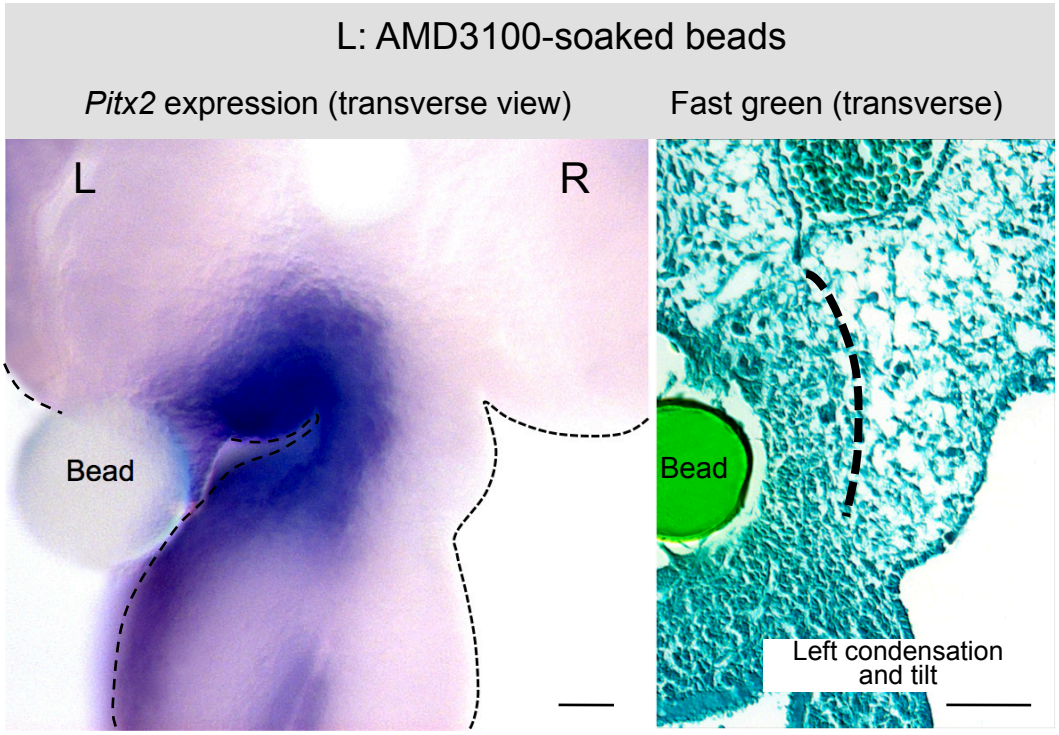
L: AMD3100-soaked beads
Pitx2 expression (transverse view)
Fast green (transverse)
L
R
Bead
Bead
Left condensation and tilt

Fig. S6

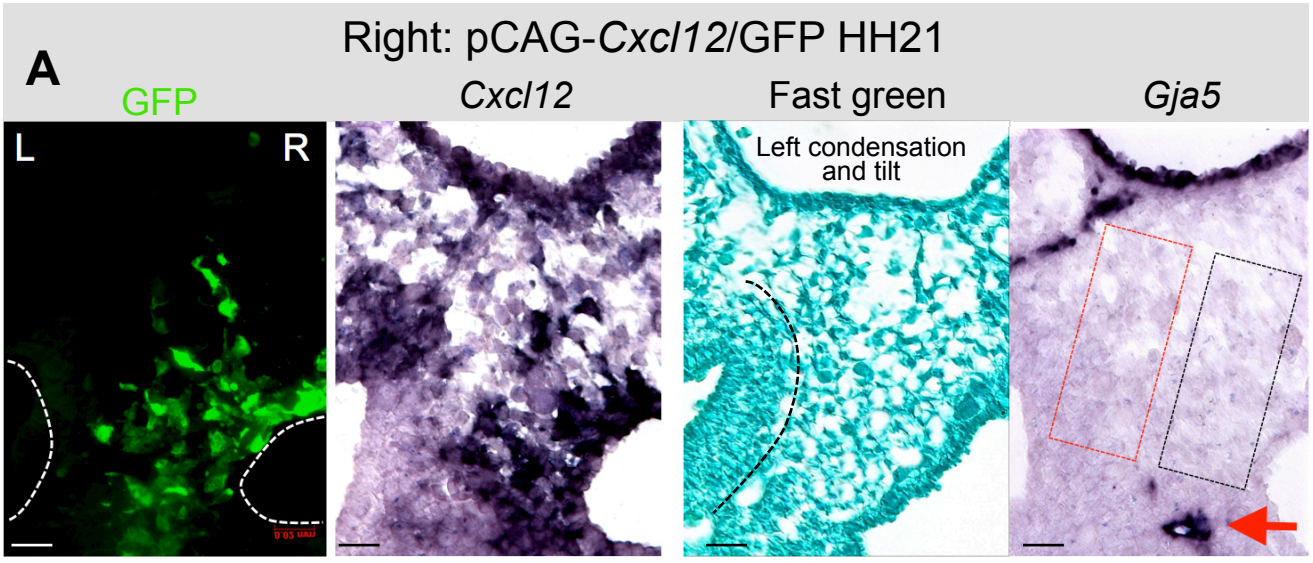
A
Right: pCAG-*Cxcl12*/GFP HH21
GFP
Cxcl12
Fast green
Gja5
L
R
Left condensation
and tilt

Fig. S6

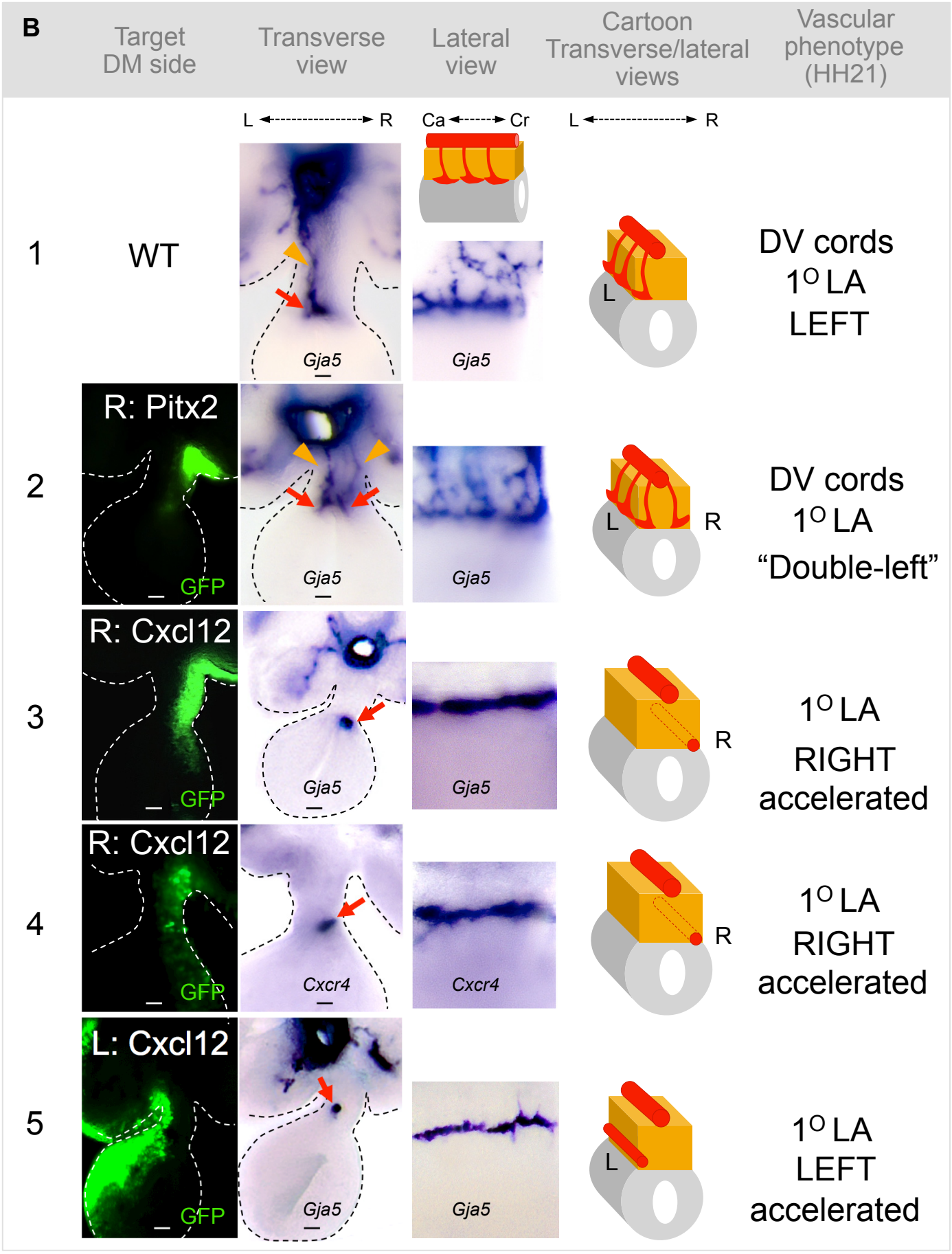
B
Target DM side
Transverse view
Lateral view
Cartoon Transverse/lateral views
Vascular phenotype (HH21)
L
R
Ca
Cr
1
WT
Gja5
DV cords
1O LA
LEFT
2
R: Pitx2
GFP
DV cords
1O LA
"Double-left"
3
R: Cxcl12
1O LA
RIGHT
accelerated
4
Cxcr4
1O LA
RIGHT
accelerated
5
L: Cxcl12
1O LA
LEFT
accelerated

Fig. S6

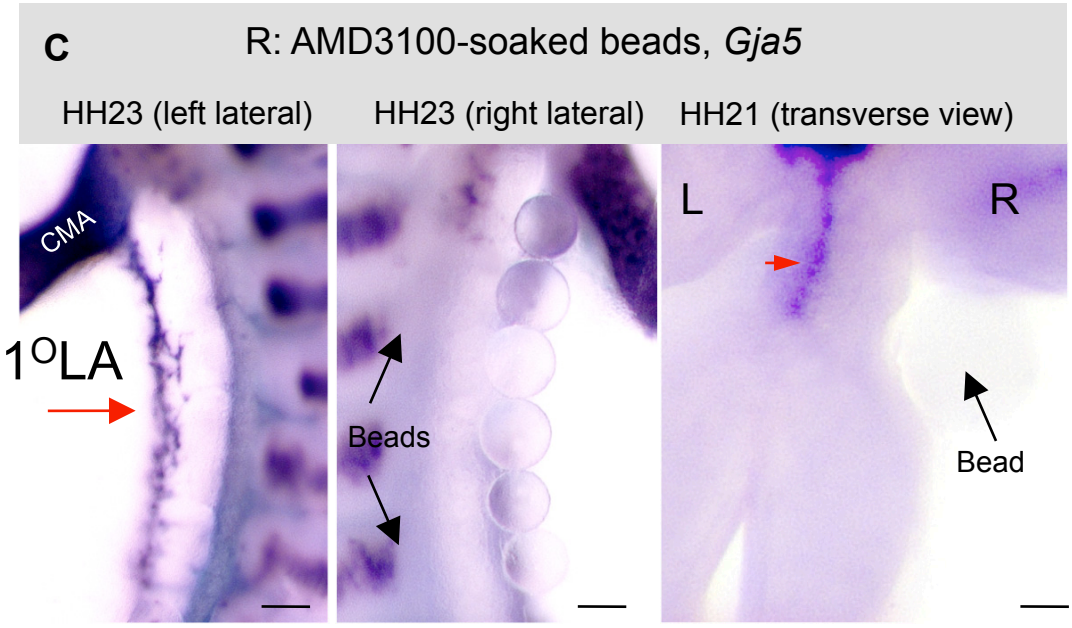
c
R: AMD3100-soaked beads, *Gja5*
HH23 (left lateral)
HH23 (right lateral)
HH21 (transverse view)
CMA
1°LA
Beads
L
R
Bead

Fig. S7

E13.5, transverse section (Prox1-GFP mouse)

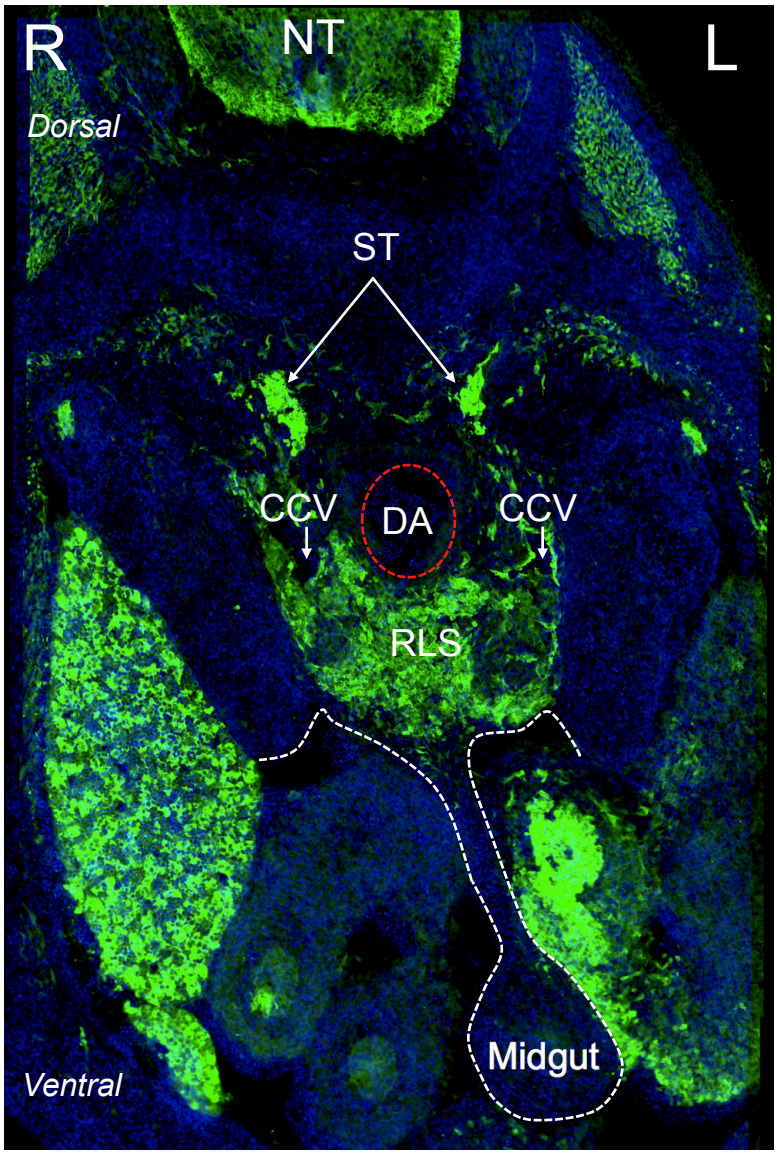

Fig. S7

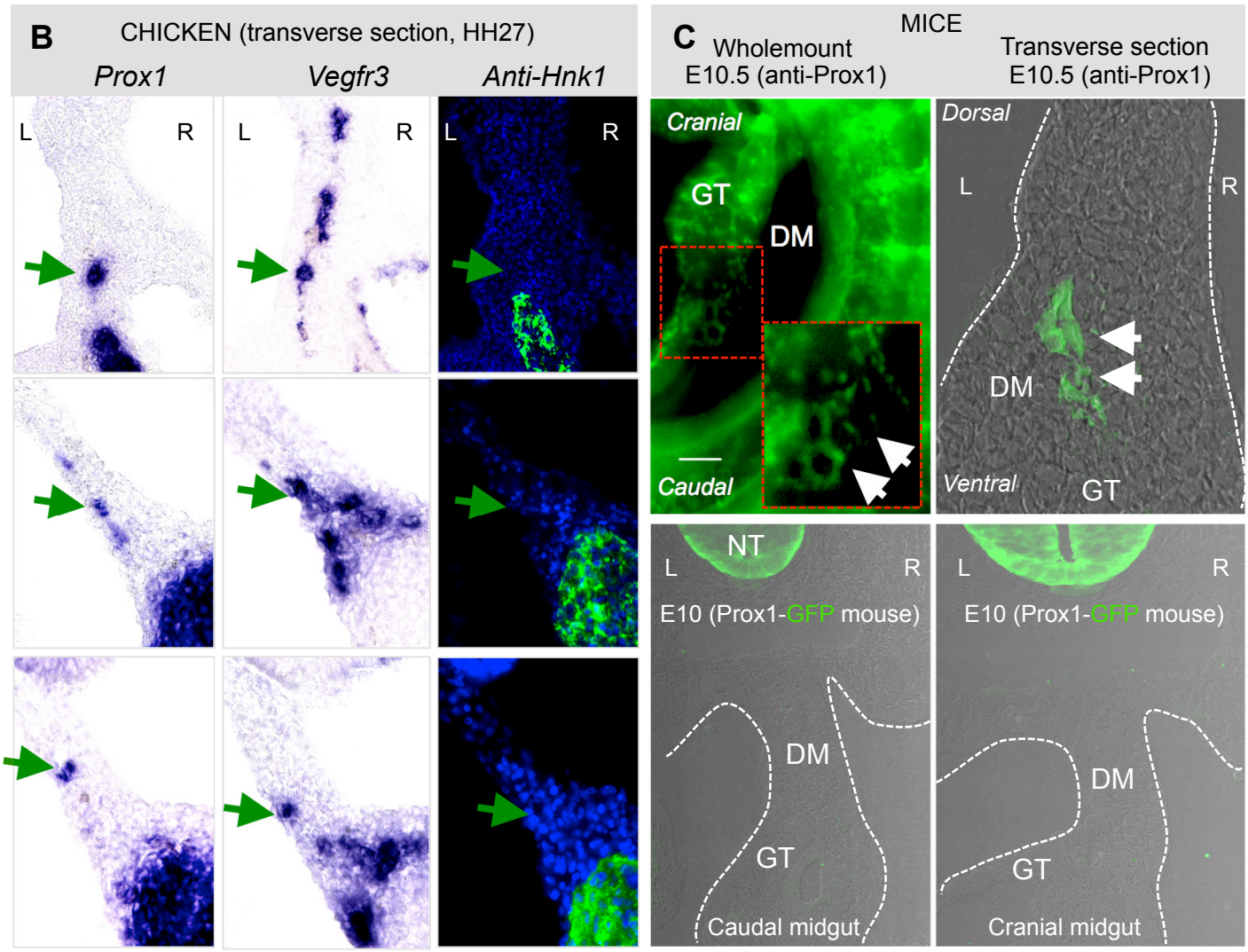
B
CHICKEN (transverse section, HH27)
Prox1
Vegfr3
Anti-Hnk1
L
R
C
MICE
Wholemount
E10.5 (anti-Prox1)
Transverse section
E10.5 (anti-Prox1)
Cranial
Caudal
GT
DM
Dorsal
Ventral
NT
E10 (Prox1-GFP mouse)
Caudal midgut
Cranial midgut

Fig. S8

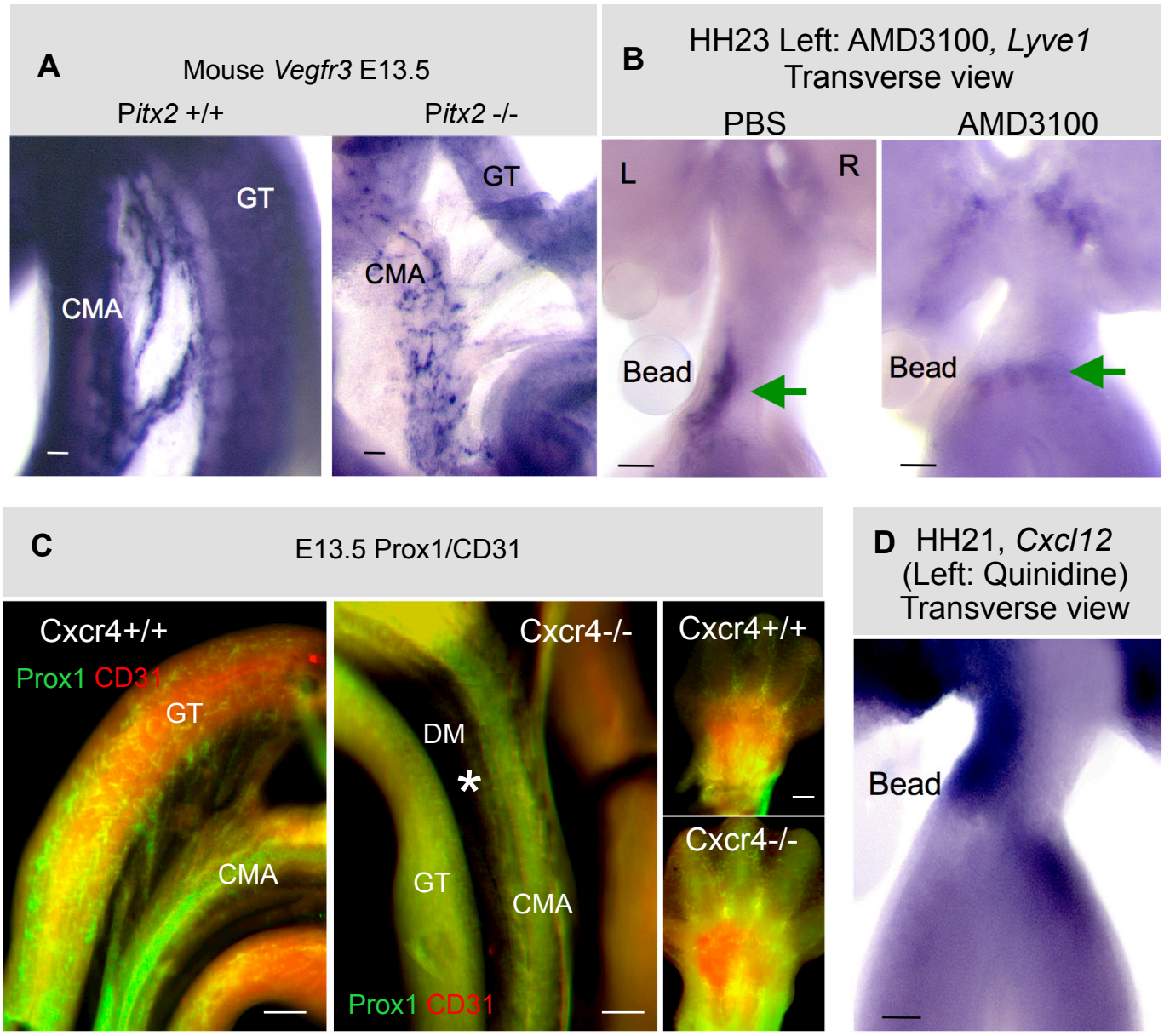
A
Mouse *Vegfr3* E13.5
Pitx2 +/+
Pitx2 -/-
GT
CMA
GT
CMA
B
HH23 Left: AMD3100, *Lyve1*
Transverse view
PBS
AMD3100
L
R
Bead
Bead
C
E13.5 Prox1/CD31
Cxcr4+/+
Prox1 CD31
GT
CMA
Cxcr4-/-
DM
*
GT
CMA
Prox1 CD31
Cxcr4+/+
Cxcr4-/-
D
HH21, *Cxcl12*
(Left: Quinidine)
Transverse view
Bead